Atmos. Chem. Phys., 8, 6453–6468, 2008
www.atmos-chem-phys.net/8/6453/2008/

Atmospheric Chemistry and Physics

Evaluation of 1,3,5 trimethylbenzene degradation in the detailed tropospheric chemistry mechanism, MCMv3.1, using environmental chamber data

A. Metzger[1], J. Dommen[1], K. Gaeggeler[1], J. Duplissy[1], A. S. H. Prevot[1], J. Kleffmann[2], Y. Elshorbany[2], A. Wisthaler[3], and U. Baltensperger[1]

[1]Laboratory of Atmospheric Chemistry, Paul Scherrer Institut, 5232 Villigen, Switzerland
[2]Physikalische Chemie/FB C, Bergische Universität Wuppertal, 42097 Wuppertal, Germany
[3]Institut für Ionenphysik, Universität Innsbruck, 6020 Innsbruck, Austria

Received: 10 April 2008 – Published in Atmos. Chem. Phys. Discuss.: 11 June 2008
Revised: 11 September 2008 – Accepted: 21 September 2008 – Published: 13 November 2008

Abstract. The degradation mechanism of 1,3,5-trimethylbenzene (TMB) as implemented in the Master Chemical Mechanism version 3.1 (MCM) was evaluated using data from the environmental chamber at the Paul Scherrer Institute. The results show that the MCM provides a consistent description of the photo-oxidation of TMB/NO_x mixtures for a range of conditions. In all cases the agreement between the measurement and the simulation decreases with decreasing VOC-NO_x ratio and in addition with increasing precursor concentration. A significant underestimation of the decay rate of TMB and thus underestimation of reactivity in the system, consistent with results from previous appraisals of the MCM, was observed.

Much higher nitrous acid (HONO) concentrations compared to simulations and expected from chamber characterization experiments were measured during these smog chamber experiments. A light induced NO_2 to HONO conversion at the chamber walls is suggested to occur. This photo-enhanced NO_2 to HONO conversion with subsequent HONO photolysis enhances the reactivity of the system. After the implementation of this reaction in the model it describes the decay of TMB properly. Nevertheless, the model still overpredicts ozone at a later stage of the experiment. This can be attributed to a too slow removal of NO_2. It is also shown that this photo-enhanced HONO formation is not restricted to TMB photo-oxidation but also occurs in other chemical systems (e.g. α-pinene). However, the influence of HONO as a source of OH radicals is less important in these more reactive systems and therefore the importance of the HONO chemistry is less obvious.

Correspondence to: J. Dommen
(josef.dommen@psi.ch)

1 Introduction

Volatile organic compounds (VOC) are emitted into the atmosphere from anthropogenic and biogenic sources. Aromatics are mostly emitted by fuel combustion and evaporation and will therefore influence mainly urban areas where they contribute 16–44% to the total hydrocarbon mass emitted into the atmosphere (Calvert et al., 2002; Derwent et al., 2000; Molina et al., 2007). Thus they contribute significantly to the production of ozone and other secondary pollutants in these areas. Special attention has been paid to the ability of aromatics to form secondary organic aerosol (SOA) and its effect on human health and the environment/climate. Even in urban areas more than 60% of the total organic aerosol mass can be attributed to SOA (Lanz et al., 2007).

The most abundant aromatic hydrocarbons are alkyl benzenes such as toluene, xylenes, trimethylbenzenes and their analogues (Calvert et al., 2002). In recent years research has been quite active to better understand and describe the degradation of aromatic hydrocarbons. The Master Chemical Mechanism (MCM) is an almost explicit chemical mechanism describing the degradation of a large number of VOCs. The mechanism construction protocol is described in a series of publications (Jenkin et al., 1997, 2003; Saunders et

al., 2003a). The aromatic mechanism as represented in the MCM was recently updated (Bloss et al., 2005b) and evaluated against environmental chamber data during the EXACT project (Bloss et al., 2005a). Although the updated mechanism shows improved ability to model these European Photoreactor (EUPHORE) experiments, significant deficiencies in the aromatic mechanism remained. It was shown that in general the mechanism tends to over-predict the ozone formation and to underestimate the reactivity in the system (Bloss et al., 2005a). This is conflicting as one could reduce the ozone formation by reducing the RO_2 concentration which limits the conversion of NO to NO_2 but this will also lead to a reduction in OH formation and thus of reactivity. Therefore, the challenge is to find a chemical process that enhances the reactivity of the system without increasing the NO to NO_2 conversion rate.

Due to the well defined conditions under which smog chamber experiments can be performed, they are highly valuable for the development and evaluation of chemical mechanisms and to get a better understanding of processes leading to SOA formation. There have been a number of studies evaluating the Master Chemical Mechanism against data of different compounds from various environmental chambers e.g. aromatics, including TMB (Bloss et al., 2005a; Wagner et al., 2003), ethene (Zador et al., 2005), isoprene and its oxidation products (Pinho et al., 2005) as well as various alkenes (Hynes et al., 2005; Pinho et al., 2006) and monoterpenes (Pinho et al., 2007; Saunders et al., 2003b). Usually chamber experiments are performed using higher concentrations than found in the atmosphere. Therefore it was shown that $O(^3P)$ reactions become important under chamber conditions which are negligible in the atmosphere (Hynes et al., 2005; Pinho et al., 2005, 2006 2007). Sensitivity studies showed that wall reactions as well as uncertainties in the photolysis rates can significantly influence the system under observation (Bloss et al., 2005a, b; Carter et al., 2005; Hynes et al., 2005; Pinho et al., 2005).

In this paper we describe the evaluation of the Master Chemical Mechanism of 1,3,5-trimethlybenzene photooxidation using the data from the Paul Scherrer Institute (PSI) chamber. In addition, experiments conducted in the Statewide Air Pollution Research Center (SAPRC) chambers are also evaluated to confirm our measurements. We substantially extend the number of experiments and variations of experimental conditions for aromatics compared to previous studies in the EUPHORE (Bloss et al., 2005a). We also consider the sensitivity of the reaction system to chamber wall reactions and evaluate mechanistic variations reported in literature. We propose a photo-enhanced conversion of NO_2 to HONO on the chamber walls in the presence of VOCs to be responsible for part of the discrepancies between model and measurements.

2 Experimental

2.1 Reaction chamber

Details of the indoor PSI chamber, the experimental setup and the instrumentation are extensively described elsewhere (Paulsen et al., 2005). Briefly, photo-oxidation experiments were carried out in the 27 m^3 FEP chamber at ∼20°C and ∼50% relative humidity (RH). The chamber was first humidified before introducing NO and NO_2. A known amount of the compound of interest (1,3,5-trimethylbenzene, Fluka, 99.5%) was evaporated in a heated glass sampling bulb and flushed with pure air into the chamber where it was allowed to equilibrate for 30 min. Four xenon arc lamps were used to simulate the solar light spectrum and start the photochemistry.

2.2 Instrumentation

TMB and its oxidation products were monitored using proton-transfer-reaction mass spectrometry (PTR-MS, Ionicon Analytik GmbH, Austria). The sensitivity of the instrument was determined using several gas standards (Apel & Riemer Environmental Inc., USA) containing TMB and a total of 27 alcohols, ketones, and aldehydes. For compounds for which a standard was available an uncertainty of 5% was attributed to the data. For all compounds for which no authentic standards were available an average sensitivity, derived from the available calibrations was applied to the data. The associated uncertainty of 30% was attributed to these measurements.

Ozone was measured by UV absorption with a commercial Environics S300. NO and NO_2 were quantified with a Thermo Environmental Instruments 42C trace level, which was equipped with a photolytic converter (Blue light Converter of Droplet Measurements Technologies, Boulder, CO) to selectively reduce NO_2 to NO. The latter was then detected by NO+O_3 chemiluminescence. Formaldehyde (HCHO) was measured with the Hantzsch method as described by Kelly and Fortune (1994) and discussed in Hak et al. (2005) or Steinbacher et al. (2004) (Supplementary Information http://www.atmos-chem-phys.net/8/6453/2008/acp-8-6453-2008-supplement.pdf).

2.2.1 Nitrous acid (HONO) measurements

The measurement of HONO is quite complex and needs either additional instrumentation or a special setup of the instruments running at the PSI chamber. Therefore only a limited number of experiments with HONO data are available, among them six TMB experiments. Several methods to measure nitrous acid were applied.

For a set of experiments, a Long Path Absorption Photometer (LOPAP), which is described in detail elsewhere (Heland et al., 2001; Kleffmann et al., 2002) was used.

Briefly, HONO is sampled in a stripping coil by a fast chemical reaction and converted into an azo-dye which is photometrically detected by long-path absorption inside a special Teflon tube. The technique was successfully validated with the DOAS technique under field and smog chamber conditions (Kleffmann et al., 2006).

As the LOPAP instrument was only available for a short period the PTR-MS technique was expanded to the measurement of gaseous nitrous acid. HONO was measured in its dehydrated form [MH^+-H_2O] (m/z 30). The standard settings of the instrument were changed to reduce the high signal background of m/z 30 which is a result of the reaction of N_2 and O_2 in the ion source producing NO^+. The signal shows interference towards HONO formation from NO_2 on the surface of the inlet and the drift tube of the PTR-MS instrument. Therefore, a Na_2CO_3 scrubber was intermittently placed in front of the inlet to selectively scrub out HONO and derive the NO_2 interference. HONO was calculated from the difference between signals with and without the scrubber (Wisthaler et al., 2005).

In parallel to the PTR-MS technique a wet effluent diffusion denuder (WEDD) coupled to an ion chromatography – mass spectrometry (IC-MS) system was also used. Briefly, air was aspired through a membrane-based parallel plate denuder (Takeuchi et al., 2004). The air flow rate was set to 1 L/min and samples were taken for 0.5 h. The water (Millipore, Milli-Q, 18 MΩ×cm) was continuously pumped through the denuder at a flow rate of 0.5 ml/min at counter flow to the air. The water flows through the two denuders were each collected and concentrated on a trace concentrator column (TAC-LP1, Dionex) and were then analyzed using (IC-MS) in a quasi-continuous fashion. The mass spectrometer (MSQ, Dionex) has a single quadrupole mass detector and uses the atmospheric pressure ionization (API) technique which is operated using electrospray ionization (ESI). To test possible interferences two denuders were connected in series. As the measurements suffer from interferences (Gutzwiller et al., 2002) the method was only applied for experiments with low initial precursor concentrations and for cross calibrations of the PTR-MS technique using a pure HONO source (see Supplementary Information http://www.atmos-chem-phys.net/8/6453/2008/acp-8-6453-2008-supplement.pdf).

2.3 Overview of the available experiments

A list of TMB photo-oxidation experiments, along with the range of initial conditions is given in Table 1. In addition to the experiments from our laboratory, experimental results from the SAPRC indoor chambers (Carter et al., 1995b) were also used in the evaluation. Measurements from the Dividable Teflon Chamber (DTC) and the Xenon Arc Teflon Chamber (XTC) are included. Similar to our chamber these are built in Teflon, but are somewhat smaller with a volume of around 5 m^3 and a surface-to-volume ratio (S/V) of roughly 3.5 (e.g. Carter, 2000) (PSI: 27 m^3, S/V=2). The DTC chambers are illuminated by blacklights. The available datasets from these chambers were used previously in the development and evaluation of the SAPRC-99 mechanism (Carter, 2000), and in the previous appraisals of the isoprene, butane and alkene as well as α- and β-pinene degradation (Pinho et al., 2005, 2006, 2007). For the simulations in this study we used the auxiliary mechanism of each of the chambers as described in Carter et al. (1995a) and updated by Pinho et al. (2005).

Table 1. List of 1,3,5-trimethylbenzene experiments with the ranges of initial concentrations, VOC/NO_x ratio and relative humidity.

	PSI	CTC[b]	DTC[b]
No. of available runs	53	4	7
TMB (ppb)	76–1243	170–330	80–340
NO_x (ppb)	43–912	260–520	130–560
VOC/NO_x	0.33–16[a]	0.71–0.7	0.3–1.3
RH %	46–68	<5	<5

[a] For the high VOC/NO_x experiments HONO was used as replacement NO_x where HONO was continuously flushed into the chamber, so that a steady state NO_x concentration of around 8 ppb was reached.
[b] SAPRC indoor chambers. CeCERT Xenon Arc Teflon Chamber (CTC, 6 m^3) and Dividable Teflon Chamber (DTC, 5 m^3, blacklights).

2.4 Chemistry of the TMB photo-oxidation as represented in the MCM

The complete degradation scheme of TMB through to CO_2 and H_2O in the MCM-v3.1 contains 389 reactions and 145 products. The methodology of the construction of the aromatic mechanism is described in Jenkin et al. (2003). This version was recently updated and tested against environmental chamber experiments as part of the EXACT project (Bloss et al., 2005a, b).

The oxidation pathways of TMB to first generation products in the presence of NO_x, as implemented in the MCMv3.1, are shown in Fig. 1. H-abstraction from a methyl-group leads to the formation of 3,5-dimethylbenzaldehyde as a first generation product while the other channels involve addition of OH and O_2 to the aromatic ring. 2,4,6-trimethylphenol is formed by abstraction of an H-atom by O_2 from the ring or by isomerisation of the adduct formed by reaction of O_2 with the OH adduct, and elimination of HO_2. The major route involves addition of O_2 to the OH-adduct followed by a ring opening leading to the formation of methylglyoxal and the proposed co-products furanones (e.g. 3,5-dimethylfuran-2(5H)-one) and 2-methyl-4-oxopent-2-enal from the decomposition of a peroxide-bicyclic radical. Epoxy type compounds have been proposed

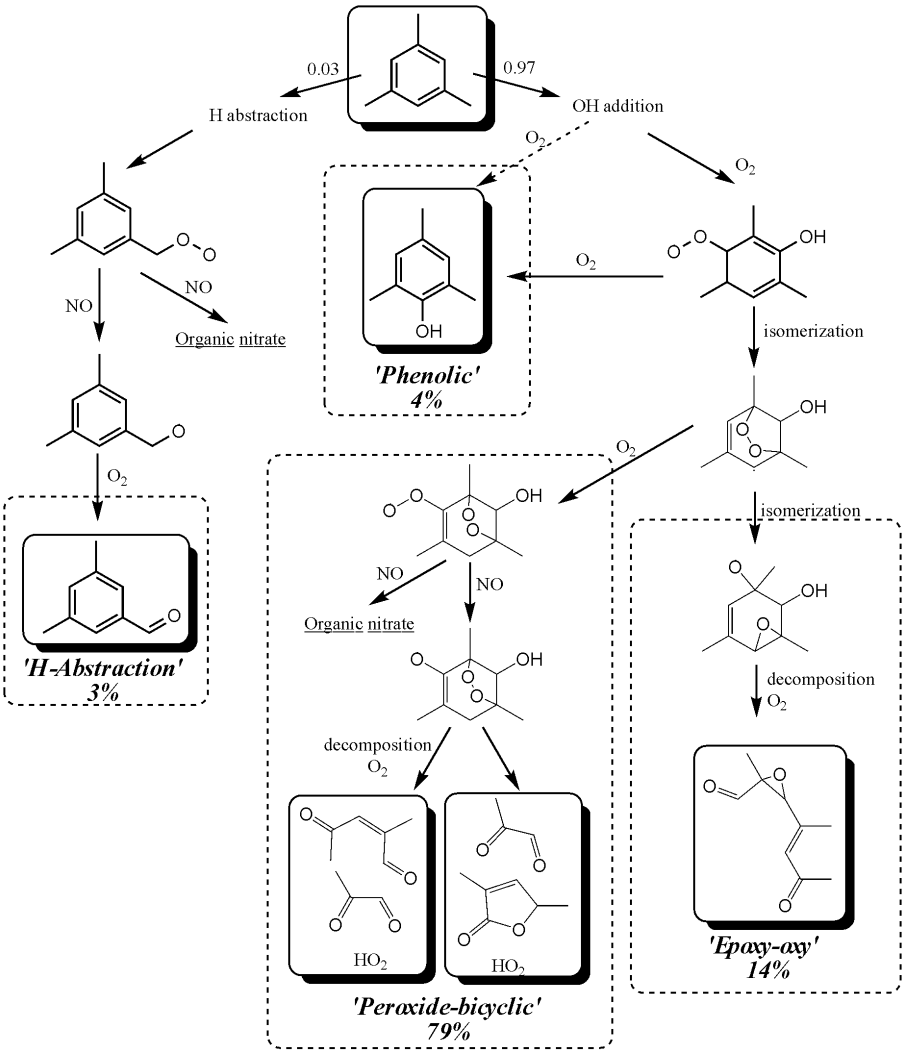

Fig. 1. Partial schematic representation of the OH-initiated oxidation of TMB as implemented in the MCMv3.1. The chemistry shown includes for RO_2 radicals only the reactions with NO. The first generation products are shown in boxes, and the branching ratio of the respective forming pathway is given in percent.

as oxidation products, and support for their formation was provided by product studies of Yu and Jeffries (1997). The epoxy route proceeds by formation and subsequent decomposition of a cyclic epoxy-oxy-radical, and is included to represent the balance of the chemistry not accounted for by other routes.

The further degradation of the first and subsequent generation products is also represented in MCM v3.1, as are competitive reactions of the intermediate peroxy radicals formed at each stage, which gain importance as NO_x is consumed (see Bloss et al., 2005b; Jenkin et al., 2003).

3 Characterization of the PSI chamber

In chamber studies, attention has to be paid to external factors that influence the chemical system under observation, mainly the light source and reactions that occur at the wall of the chamber. These are described in the following.

3.1 Photolysis processes

The rates of photolysis processes depend on the intensity and spectral distribution of the light source. Spectral distributions are based on spectrometer measurements (Bentham Spectrograph DMc 150 FC), whereas absolute light intensities were determined by NO_2 actinometry experiments (Paulsen et al., 2005). The time trend of the light intensity was tracked using $J(NO_2)$ filter radiometer (FR) data and regular NO_2 actinometry experiments. The light intensity measured by NO_2 actinometry and $J(NO_2)$-FR stayed constant ($\pm$4%) over the time period considered. An uncertainty of $\pm$12% was attributed to the $J(NO_2)$ value measured with chemical actinometry.

Table 2. Reactions that were included in the auxiliary mechanism to represent chamber dependent processes and $J(NO_2)$ along with their respective parameters and uncertainties. As noted, parameters are either derived from experiments or adopted from literature.

	Process	Parameter	Upper/lower limits	Notes
1	$h\nu$+wall→HONO (g)	9.1×10^6 molecule cm^{-3} s^{-1}	5×10^6–13×10^6 molecule cm^{-3} s^{-1}	PSI chamber characterization/measured
2	$[HONO]_0$ (g)	$[HONO]_0 = 0.0074\times RH + 0.006\times [NO_2]_0$	0–3 ppb	PSI chamber characterization/measured
3	NO_2 (g)→0.5 HONO (g)+0.5 $w$$HNO_3$ (ads)	0.53×10^{-6} s^{-1}	2.1×10^{-7} to 4.2×10^{-6} s^{-1}	PSI chamber characterization/measured Expressed as HONO formation rate!
4	$h\nu$+wall→HCHO (g)	5×10^6 molecule cm^{-3} s^{-1}	2.5×10^6–1×10^7 cm^{-3} s^{-1}	PSI chamber characterization/measured
5	N_2O_5 (g)→2 $w$$HNO_3$ (ads)	1×10^{-5} s^{-1}	5×10^{-6}–4.7×10^{-5} s^{-1}	Adopted from (Carter and Lurmann, 1991) and (Bloss et al., 2005a)
6	N_2O_5 (g)+H_2O (g)→2 $w$$HNO_3$ (ads)	1×10^{-20} cm^3 s^{-1}	1.1×10^{-23}–1.3×10^{-19} cm^3 s^{-1}	
7	OH (g)+X (g)→HO_2 (g)+X (g)	$k_{(OH+CO)}$	–	PSI chamber characterization/measured
7a	$[X]_0$ (g)	300 ppb	100–600 ppb	
8	O_3 (g)→$w$$O_3$ (ads)	4×10^{-6} s^{-1}	2×10^{-6}–8×10^{-6} s^{-1}	PSI chamber characterization/measured
9	HNO_3 (g)→$w$$HNO_3$ (ads)	1×10^{-4} s^{-1}	5×10^{-5}–2×10^{-4} s^{-1}	Adopted from (Bloss et al., 2005a)
10	$w$$HNO_3$ (ads)+$h\nu$→NO_2 (g)+OH (g)	J_{HNO_3}	(0–2)J_{HNO_3}	
11	all species (g)$\overset{\text{dilution}}{\longrightarrow}$	k_{dilution}=flow/volume	±10%	PSI chamber characterization /measured
12	$J(NO_2)$		±12%	PSI chamber characterization/measured

The photolysis rates were determined from the measured light spectrum and using the absorption cross sections and quantum yield data summarized by Jenkin et al. (1997) for the MCM. The rates of a number of photolysis reactions were updated according to Pinho et al. (2005).

3.2 Chamber auxiliary mechanism

An extensive characterization of chamber dependent chemical surface reactions was performed, which is a prerequisite to simulate the photochemical reactions of any chemical species in a smog chamber. The relevant parameters for an auxiliary mechanism of our chamber were determined using clean air (number of experiments N=12), NO_x-air (N=2), CO-air (N=4) and CO-NO_x-air (N=3) irradiations. In recent studies chamber related reactions occurring at the Teflon wall of a chamber have been discussed in detail and form the basis for the reactions used in this study (Bloss et al., 2005a; Carter et al., 2005; Finlayson-Pitts et al., 2003; Hynes et al., 2005; Rohrer et al., 2005; Zador et al., 2006). The relevant reactions are listed in Table 2.

One of the most important and controversially discussed chamber artifacts is the enhanced background reactivity in simulation chambers under illuminated conditions (Killus and Whitten, 1990). In the study of Rohrer et al. (2005) HONO was clearly identified for the first time to explain the photo-enhanced background reactivity. HONO is released from the walls and its photolysis enhances the OH radical production (Rohrer et al., 2005; Zador et al., 2006). In order to quantify the light induced HONO production in our chamber, model calculations were performed using a simple NO_x/HONO/CO/HCHO reaction scheme downloaded from the MCM website to describe CO-air and pure air experiments. Reactions to account for wall processes were included (Table 2). For experiments, where HONO measurements were available, the model was constrained with the measured HONO concentrations and therefore the light induced HONO wall production rate $W(\text{HONO})$ could be derived, according to Eq. 1 (Zador et al., 2006).

$$W(\text{HONO}) = \frac{d[\text{HONO}]}{dt} - k_{\text{OH+NO}}[\text{OH}][\text{NO}] - k_{\text{NO}_2+\text{wall}}[\text{NO}_2] + [\text{HONO}]_{\text{obsserved}}(k_{\text{OH+HONO}}[\text{OH}] + J(\text{HONO})) \quad (1)$$

Thus $W(\text{HONO})$ is given by the gradient of the observed HONO concentration and the sources (negative terms) and sinks (positive terms) of HONO. Sources are the production via NO+OH reaction and the heterogeneous hydrolysis of NO_2 at the chamber walls, while the loss is given by the photolysis and the reaction with OH.

The error due to the uncertainty in the calculation of $J(\text{HONO})$ and the measurement of HONO was estimated to be 15%. When no HONO data was available, the auxiliary mechanism was tuned to describe the observed NO, NO_2 and O_3 formation in pure air, CO/air and CO/NO_x/air experiments. A mean value of the HONO formation rate of 22 ppt/min±40% (1σ) was determined from 17 chamber characterization runs during the period considered. The variation was determined by the history of the chamber. In the work of Rohrer et al. (2005) and Zador et al. (2006) it was shown that the light induced HONO off-gassing depends on temperature, RH and the photolysis rate of NO_2. Due to the lack of experimental variability no dependence on the temperature and RH could be derived here. Application of the SAPHIR parameterization using the higher (lower) of

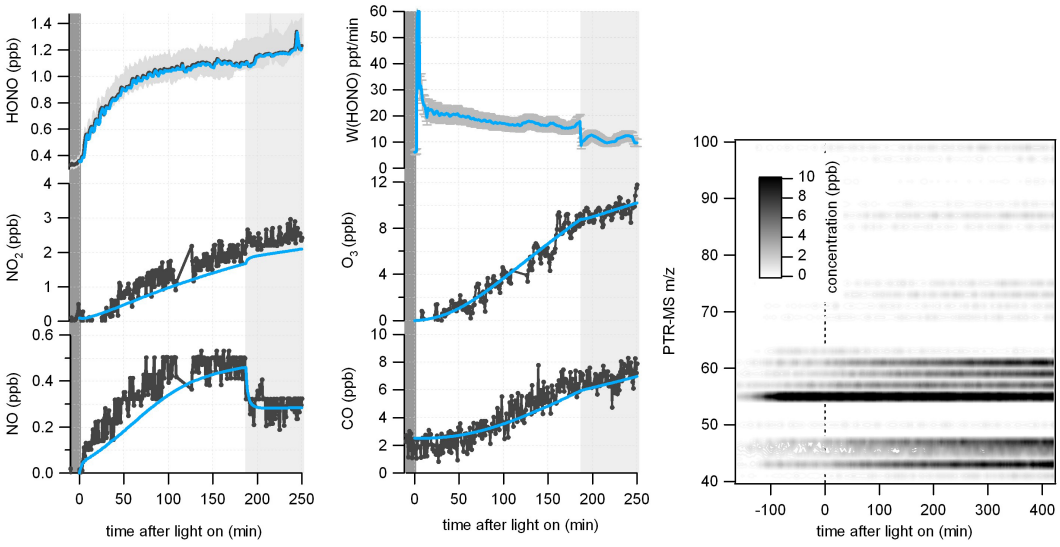

Fig. 2. Concentration time profiles of HONO, NO_x, O_3 and CO for a pure air chamber experiment. Dark grey lines show measured values while the blue lines show the result of a model calculation. The middle top panel shows the HONO production rate W(HONO) in ppt/min as derived from measurement/model calculations (see text). After 190 min the light intensity was reduced to 50% (grey shaded area). Right panel: PTR-MS mass traces vs. time.

their two parameter sets would yield a HONO off-gassing rate of $7.4\times10^6\,s^{-1}$ ($4\times10^6\,s^{-1}$) for typical experimental conditions in the PSI chamber (293 K, $J(NO_2)$=0.0016 s^{-1}, RH=50%, surface-volume-ratio=2). This is similar to our experimental value of $9\times10^6\,s^{-1}$ while for the EUPHORE chamber this rate is reported to be around one order of magnitude higher (Zador et al., 2006).

An initial HONO concentration needs to be included to simulate the small increase of HONO during the humidification process (see Fig. 2) in the dark chamber and the increase of HONO after the NO_x input. This depends on the initial NO_x level and the history of the chamber. Typically HONO increases during humidification up to around 0.4 ppb. Immediately with the NO_x input the HONO concentration rises depending on the amount of NO_x added. Therefore an empirical formula was used to describe the initial HONO concentration:

$$[\mathrm{HONO}]_0 = 0.0074 \times \mathrm{RH} + 0.006 \times [\mathrm{NO_2}]_0\,. \qquad (2)$$

The initial HONO concentration mainly influences the reactivity in the beginning of the experiment. Typical values range between 0.8 and 3 ppb for the experiments considered.

The heterogeneous dark reaction $NO_2 \rightarrow 0.5$ HONO+0.5 HNO_3 was studied and discussed in detail in a review article of (Finlayson-Pitts et al., 2003). Rate constants reported in this study range from 2.1×10^{-7} to $4.2\times10^{-6}\,s^{-1}$ (normalized to a surface- volume ratio of 2). An even higher value of $2.3\times10^{-5}\,s^{-1}$ was used for studies at the EUPHORE chamber (Bloss et al., 2005a). The rate of this reaction for our chamber was determined from NO_2 dark loss measurements (N=4) at different initial NO_2 concentrations. An optimal rate was found to be $(1.05\pm0.35)\times10^{-6}\,s^{-1}$. To test the influence of this reaction on the TMB system the reaction rate was varied between the lower and upper limit given in Finlayson-Pitts et al. (2003) (see Sect. 5.1).

A light induced HCHO formation was introduced which is necessary to follow the observed HCHO production when the chamber is illuminated. HCHO serves as a radical source and influences the system mainly under low VOC conditions (Carter et al., 2005; Zador et al., 2006). Literature values range from 0.3 ppb/h (Carter et al., 2005) to 0–0.2 ppb/h (Rohrer et al., 2005) and are reported to be highest for the EUPHORE chamber with around 2 ppb/h (Zador et al., 2006). Values for our chamber are at the higher end of the reported range with 0.3–1.4 ppb/h. During pure air irradiation experiments the HO_x formation rates by HCHO are typically 1–2 orders of magnitude smaller than those from HONO photolysis.

As described in Hynes et al. (2005) N_2O_5 hydrolysis to form adsorbed HNO_3 was given with two heterogeneous reactions. According to Carter et al. (2005) this reaction is not of great importance under most conditions but is implemented for completeness. Values similar to the lower limit of Bloss et al. (2005a) were used. An O_3 wall loss of $4\times10^{-6}\,s^{-1}$was determined from experiments. Within an uncertainty of a factor of two the observed ozone production during characterization experiments is not influenced. The photolysis of adsorbed HNO_3 was included with a rate similar to the gas phase photolysis rate $J(HNO_3)$. A HNO_3 wall loss of $1\times10^{-4}\,s^{-1}$ was assumed with values taken from (Hynes et al., 2005). The off-gassing of organics from the wall that convert OH to RO_2/HO_2 leads to immediate

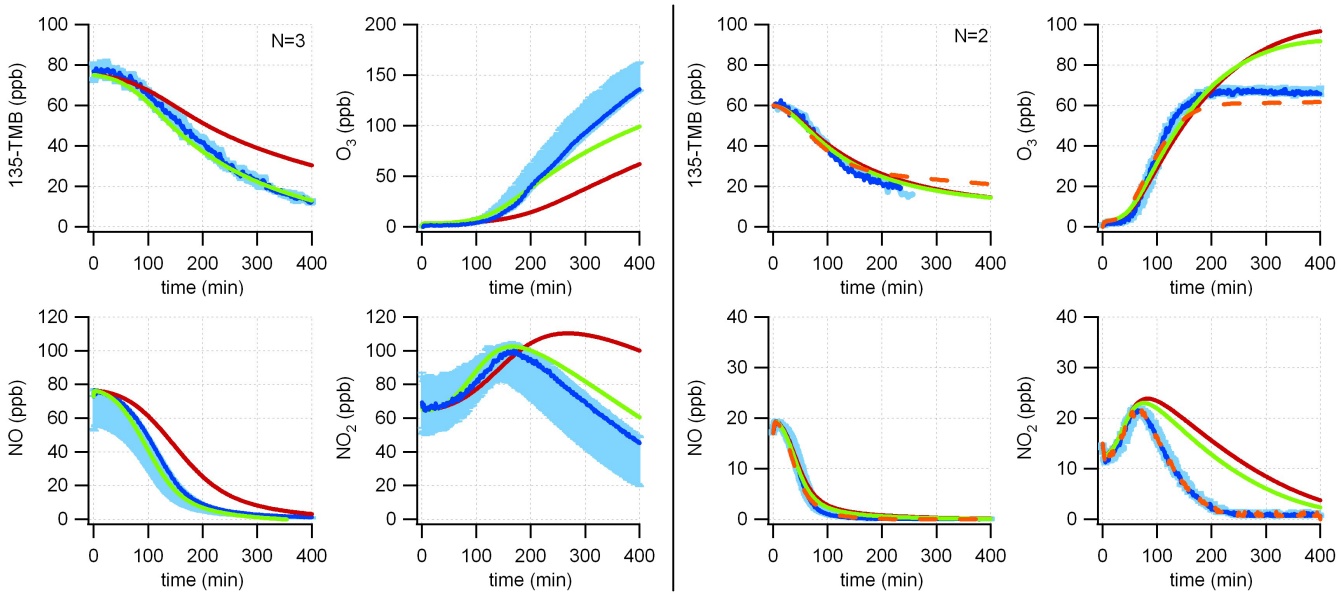

Fig. 3. Model-measurement comparison for 1,3,5-trimethylbenzene, O_3, NO and NO_2 for low concentration TMB experiments conducted at low (∼0.5, left) and medium (∼2, right) VOC/NO_x ratios. Measurement=blue, base case simulation=red, tuned mechanism=green, tuned model+constrained with measured NO_2 concentration=orange. Where different experiments with similar input concentrations were available, the average gas mixing ratios (±1 standard deviation, N=number of experiments) are indicated by the blue shaded area.

ozone formation during pure air irradiations via the conversion of NO to NO_2. A dummy reaction: OH+X→HO_2+X (with k_{OH+CO}) was included to account for this phenomenon (Rohrer et al., 2005). In order to simulate the ozone production during pure air irradiations the initial concentration of X was varied between 200 and 600 ppb. A concentration of 300 ppb was assumed for all TMB simulations.

An example of such a pure air irradiation experiment which was used to derive the light induced HONO production is shown in Fig. 2. HONO was measured with the LOPAP instrument. The determined source strength of the light induced HONO formation, W(HONO), was calculated according to Eq. 1 and is shown in the top middle panel of Fig. 2. As already discussed, during the humidification process a slight increase of HONO was observed (up to ∼370 ppt) while NO_x and O_3 stayed below the detection limit of their instruments. A slight increase in the mass traces of m/z 43, 45, 46, 57, 59, 61 as measured by PTR-MS was also observed. The increase of m/z 55 is due to an increase of the $H_3O^+(H_2O)_2$ water cluster with increasing humidity. After switching on the lights, NO, NO_2, HONO and O_3 immediately start to increase. After 190 min the light intensity was reduced to 50 %. This resulted in a new NO-NO_2 equilibrium, a reduced O_3 and CO production rate and a reduced HONO formation rate.

The derived parameters of the auxiliary mechanism could be successfully used to describe all characterization runs, although some variation in the parameters had to be taken into account, which mainly depend on the history of the chamber. The effect of these parameter uncertainties on a TMB model system is discussed in Sect. 5.3.

4 1,3,5-trimethyl benzene photo-oxidation experiments

4.1 Mechanism evaluation

A series of simulations was carried out to test the performance of the MCM against the set of different chamber experiments. Figures 3–5 show the temporal evolution of the major gas phase components for a selection of experiments conducted at molar VOC/NO_x ratios of ∼0.5 (low) and ∼2 (medium) and concentrations ranging from 60 to 1200 ppb TMB. Where different experiments with similar input concentrations were available, the average gas mixing ratios (±1 standard deviation, N=number of experiments) are indicated by the shaded area. Model runs were performed with the base case auxiliary mechanism (base). In addition a simulation is shown, where a tuning reaction (NO_2+light/surface →HONO) was implemented in the model (tuned) which describes a light-induced NO_2 conversion to HONO as discussed in a number of studies (George et al., 2005; Stemmler et al., 2006; Stemmler et al., 2007). The rate of this reaction was optimized in the way that the model is able to predict measured HONO concentrations (see below). This resulted in a single reaction rate of $8.4\times10^{-6}\,s^{-1}$ which was used for all simulations. This is a simplification of the surface

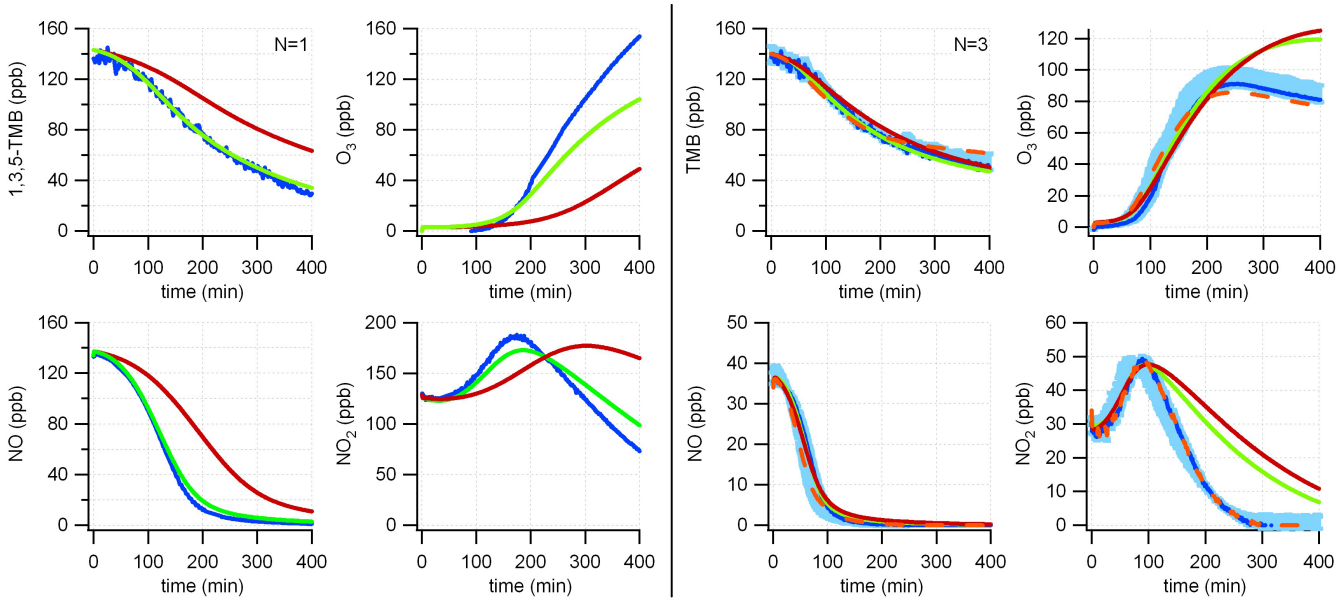

Fig. 4. Model-measurement comparison for 1,3,5-trimethylbenzene, O_3, NO and NO_2 for low-medium concentration TMB experiments conducted at low (∼0.5, left) and medium (∼2, right) VOC/NO_x ratios. Measurement=blue, base case simulation=red, tuned mechanism=green, tuned model+constrained with measured NO_2 concentration=orange.

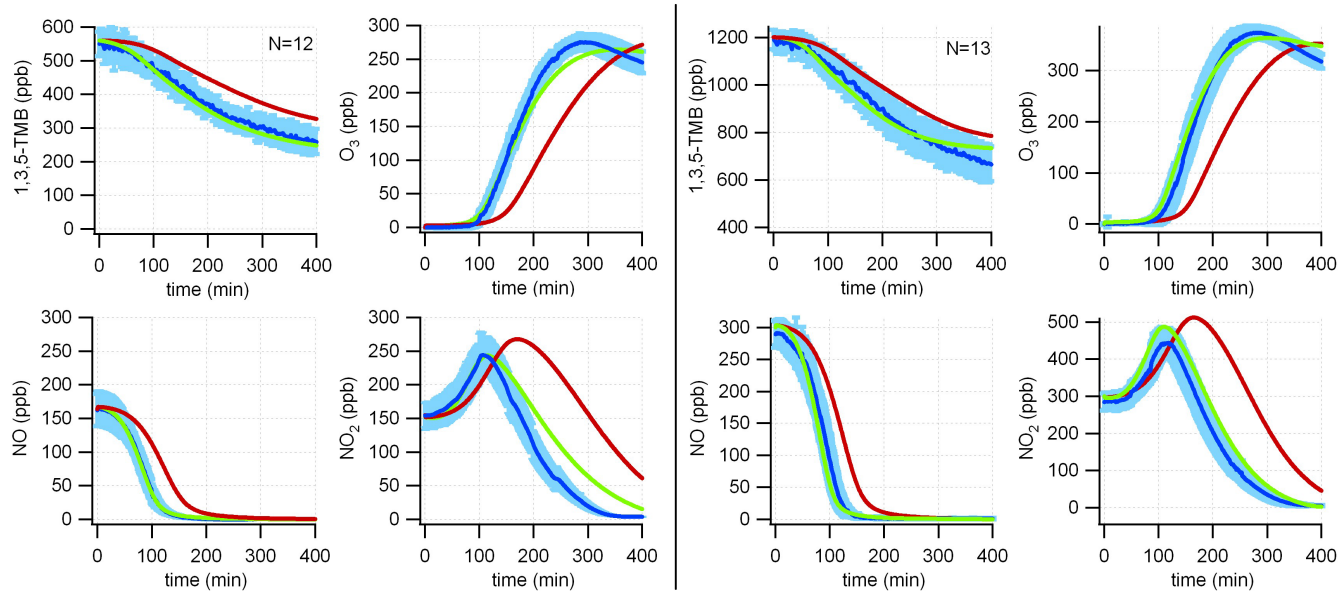

Fig. 5. Model-measurement comparison for 1,3,5-trimethylbenzene, O_3, NO and NO_2 for two sets of high concentration TMB experiments (∼600 (left) and ∼1200 ppb (right)) conducted at medium VOC/NO_x only. Measurement=blue, base case simulation=red, tuned mechanism=green. For experimental gas mixing ratios the average (±1 standard deviation) is shown for N=12 (left) and N=13 (right) experiments.

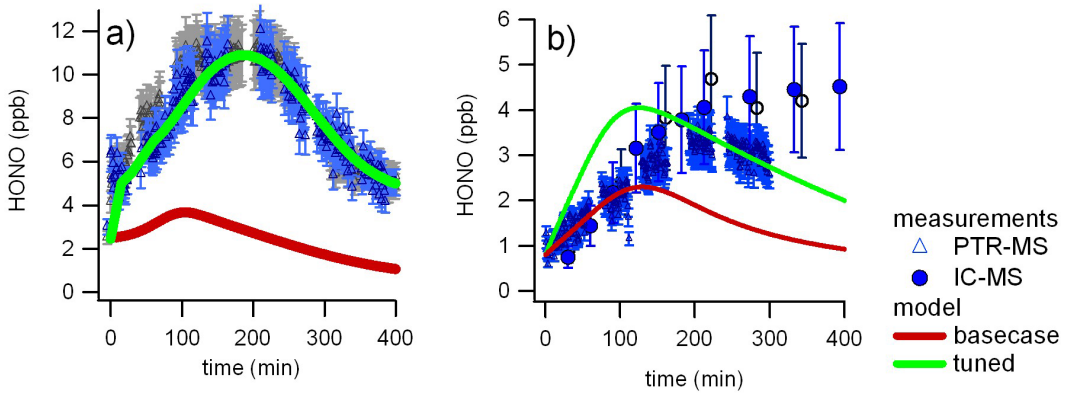

Fig. 6. Comparison of measured and modeled HONO concentrations. **(a)** shows results of 1200 ppb TMB experiments (VOC/NO_x ~2). Combined data from 2 experiments are shown, where HONO was measured with the PTR-MS. **(b)** HONO concentrations for the experiments shown in the left panel of Fig. 3 (low concentration TMB experiments/high NO_x). Combined data from three experiments are shown, where HONO was measured either with IC-MS (dark blue circles) or PTR-MS (blue triangles).

reaction, for which non-linear light- and NO_2 dependencies were observed in lab experiments. Variations of surface concentrations of adsorbed organic reactants depending on the experimental conditions applied are not considered here either. Additionally we show a tuned run where the model was constrained with the measured NO_2 concentration (tuned+NO_2 constrained).

Figures 3 and 4 show experiments with initial TMB concentrations of around 75 and 150 ppb at low (~0.5, left panel) and medium (~2, right panel) VOC/NO_x ratios. For the high NO_x experiments the base model under-predicts the TMB decay by about 100% compared to the experiment (after 400 min), pointing to a severe model under-prediction of the OH concentration. Due to the lower oxidation capacity also the NO and NO_2 conversion rate and ozone production rate are underestimated. On the other hand, under medium VOC/NO_x conditions the decay of TMB is fairly well simulated. The NO to NO_2 conversion and the ozone production are well represented by the model in the first 1.5 h, however the model starts to over-predict the NO_2 concentration followed by an over-prediction of ozone thereafter.

Figure 5 presents the base model performance for experiments conducted at medium VOC-NO_x ratios (~2) with initial TMB concentrations of 600 and 1200 ppb. While at low to medium TMB concentrations and a medium VOC/NO_x ratio (Figs. 3 and 4, right panel) the model represents comparatively well the TMB decay it starts to under-predict the reactivity of the system at higher concentrations.

Including the uniform tuning reaction into the model (NO_2+light/surface→HONO) the temporal evolution of the model simulations is significantly improved for all experimental conditions (referred to as tuned mechanism; green lines in Figs. 3–5) as the subsequent HONO photolysis acts as a source of OH radicals. As shown in Fig. 6a such an additional HONO source is necessary to match the measured HONO levels of selected experiments. While the base case simulation would significantly underestimate the measured HONO mixing ratios it is well predicted with the tuned mechanism for the 1200 ppb TMB experiment. An exception is one of the low TMB – high NO_x experiments, where the model tends to slightly overestimate the reactivity and also the measured HONO concentrations as shown in the right panel of Fig. 6b. When the model is constrained with the measured HONO concentrations the agreement improves.

The tuned mechanism also leads to a more rapid NO-NO_2 conversion and brings NO, NO_2 and O_3 in better agreement with experiments. Nevertheless, the model still underestimates the ozone levels under high NO_x conditions by around 30%. Under medium NO_x conditions the ozone concentration at the end of the experiment is basically unaffected, with an over-prediction of around 40%. If in these cases the model is constrained with measured NO_2 concentration the ozone mixing ratio is properly predicted by the model.

4.2 Product distribution

The performance of the model in simulating the concentrations of the major primary products (marked in boxes in Fig. 1) as well as formaldehyde is shown in Fig. 7 for low (left) and medium (right) VOC/NO_x ratios. Data from two single experiments are shown. The associated error bars correspond to the accuracy of the PTR-MS measurement. As described above the major oxidation pathway of TMB leads to the formation of methylglyoxal and the proposed isobaric co-products furanones (e.g. 3,5-dimethylfuran-2(5H)-one) and 2-methyl-4-oxopent-2-enal from the ring opening route. Since these cannot be distinguished by PTR-MS their predicted sum is compared with the measured m/z trace 113 (M-H^+). All primary products are fairly well simulated by the tuned mechanism especially in the first half of the experiment. Even formaldehyde, which is formed as a second and

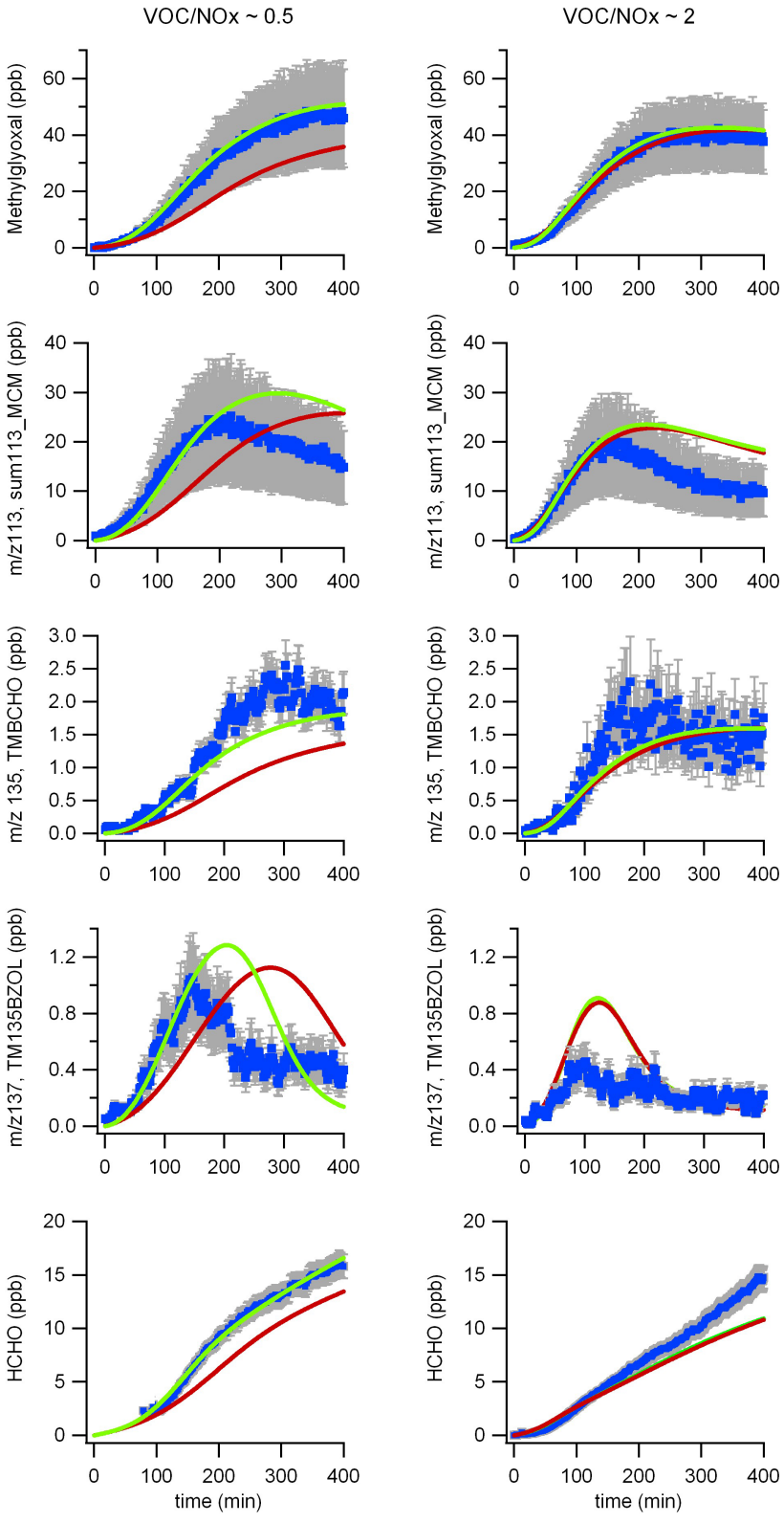

Fig. 7. Product distribution. The performance of the model in simulating the concentrations of the major primary products as well as formaldehyde for low and medium VOC-NO_x ratio is shown. Measurements (blue markers) as well as model simulations (base case=red; tuned=green). Data from two single experiments are shown. The associated error bars are due to the uncertainty in the PTR-MS calibration.

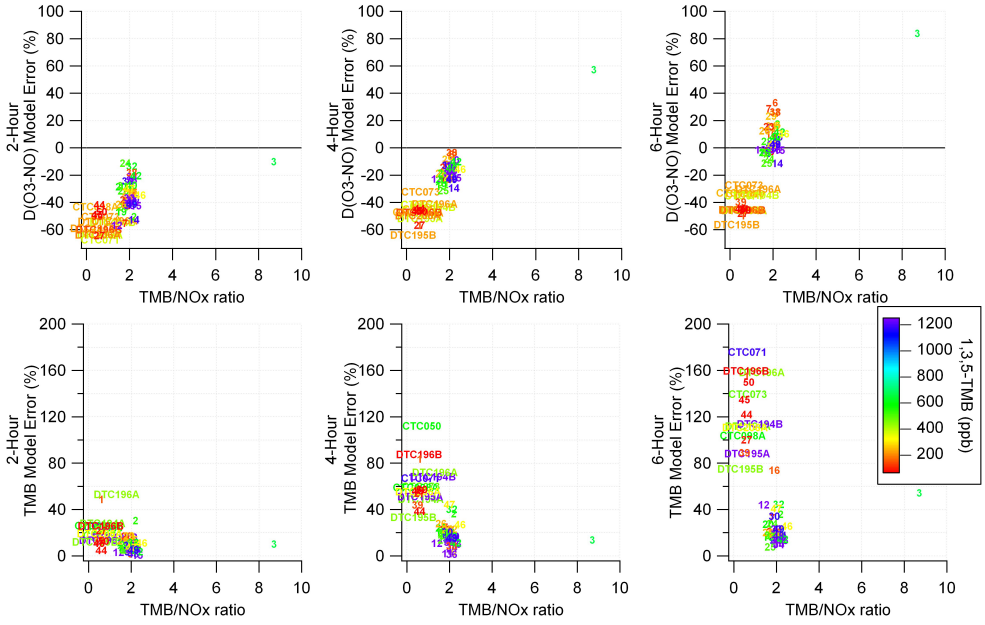

Fig. 8. Two-, four- and six-hour $D(O_3\text{-NO})$ model errors plotted vs. the initial TMB/NO_x ratio for the base case model simulation. Labels are the Run Number for the PSI experiments and the Run Label of the CTC (xenon arc chamber) and DTC (blacklight chamber) experiments of Carter (1995b). The initial TMB concentration is indicated with colors.

subsequent generation product in many steps of the aromatic mechanism, and serves as an important radical source, is well represented by the model. But especially for the m/z 113 species there is a significant discrepancy during the latter stages of the experiment. This might be an indication that the subsequent chemistry of the products is not very well known and is poorly represented in the MCM. However it should be kept in mind that an additional measurement uncertainty arises from the fact that the mass signal is not unambiguously attributable to a single compound. It might well be that the signal at m/z 113 is affected by an unknown compound or a fragment of a higher molecular weight species. Methylglyoxal and 2-methyl-4-oxopent-2-enal were identified in the aerosol phase with aerosol phase yields of 2 and 3% respectively (Healy et al., 2008). This is unlikely to affect the gas phase measurements.

4.3 Compilation of all experiments and comparison with other chambers

The precursor (TMB) decay as well as the quantity $D(O_3\text{-NO})$, which is the amount of ozone formed and NO oxidized are used as the main criteria of model performance. $D(O_3\text{–NO})$ is defined as: $D(O_3\text{–NO})=([O_3]_t-[NO]_t)-([O_3]_0-[NO]_0)$, where $[O_3]_t$, $[NO]_t$, $[O_3]_0$ and $[NO]_0$ are the concentrations at time t and the beginning of the run, respectively. It is a measure for all processes that cause ozone formation, and gives a useful measure of the reaction development, even when O_3 is suppressed by excess NO.

To summarize the behaviour of the model performance for all experiments, single error values were calculated, where the model error is defined as (100× (model value – experimental value)/experimental value) and differences in the integrated light intensity were accounted for by normalizing the time to the ratio of a standard light intensity to the light intensity of the experiment (Pinho et al., 2006). Under-prediction of the reactivity results in a negative $D(O_3\text{–NO})$ model error. In Fig. 8 the two-, four- and six-hour precursor decay model errors as well as the $D(O_3\text{–NO})$ model errors are plotted as a function of the initial TMB/NO_x ratios. The initial TMB concentration is marked in colors. The graphs summarize the experiments in the PSI chamber and the SAPRC chambers. The model errors of the TMB decay and $D(O_3\text{–NO})$ are of similar magnitude and dependence on the VOC/NO_x ratio for all chamber types. Including the tuning reaction the model error is reduced to around ±20% for all experimental conditions.

The model error in peak ozone concentration independent of the timing is shown as a function of the initial TMB/NO_x ratio in the Supplement Fig. D1. It should be noted that under high NO_x conditions the peak ozone concentration was not reached and the ozone concentration at the end of the experiment was used which could somehow bias the results. There is a clear tendency of the model to over-predict ozone concentrations at medium VOC/NO_x and low precursor concentrations. Data from the SAPRC chambers and the EUPHORE chamber show the same order of magnitude error for the different chambers and conditions.

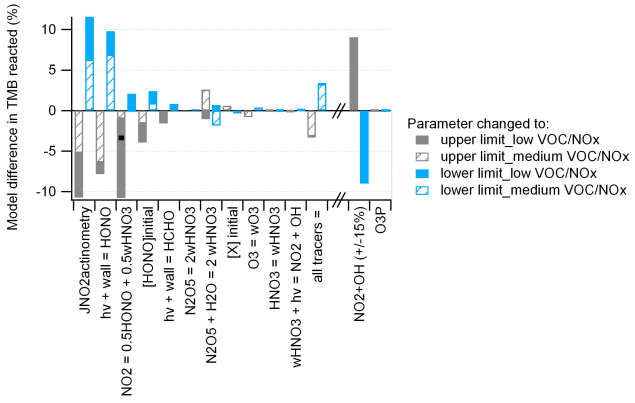

Fig. 9. TMB model sensitivity of changes of chamber related parameters like the absolute light intensity and variations in parameters of the auxiliary mechanism as described in Table 2. The relative difference (in percent) in the amount of TMB reacted after 400 min of irradiation is shown.

5 Discussion

The results demonstrate a strong dependence of the base case model performance on the initial VOC/NO_x ratio and the initial NO_x concentration. The simulations tend to increasingly under-predict the reactivity with increasing NO_x concentrations. The general under-estimation in the simulated quantities under high NO_x conditions is indicative of systematic errors in the input of radicals to the system (i.e., underestimated sources or overestimated sinks) dependent on the NO_x concentrations. On the other hand when the TMB decays are simulated better, ozone levels become strongly over-predicted. These effects are in agreement with almost all previous chamber simulations of aromatic compounds (Bloss et al., 2005a, b; Wagner et al., 2003). For TMB Bloss et al. (2005a) calculated the amount of OH radicals missing over the course of the experiment to achieve agreement between observed and modeled TMB decay to be 15% at VOC/NO_x=1 and 0.2% at VOC/NO_x=4.6. At the same time the model over-predicted the peak ozone concentration by 33 and 93% for the two cases, respectively.

SAPRC chamber experiments, all conducted at a low VOC/NO_x ratio agree well with our experiments, although the experiment to experiment variation of the SAPRC experiments is somewhat larger. The fact that a similar behavior of the mechanism performance is found for the SAPRC experiments and ours confirms our understanding and evaluation of the chamber wall reactions.

Based on the observed NO_x dependent discrepancy between model simulations and experiments we implemented a single tuning reaction (NO_2+light/surface→HONO) into the model which improved the model quality under all conditions significantly. The nature of the reaction will be discussed below.

5.1 Parameter uncertainties of the auxiliary mechanism, NO_2+OH, O(^{3}P)

The effects of chamber dependent parameters as well as possibly important kinetic and mechanistic parameters were investigated for their sensitivity on the TMB decay and thus reactivity in the system. The base case parameters as well as their minimum and maximum values are listed in Table 2 and described above. The impact of individual parameter variation in the auxiliary mechanism on the amount of TMB reacted is shown in Fig. 9. For all parameters the uncertainty is more pronounced for low VOC/NO_x conditions. Variations of the absolute light intensity, the rate of the light induced HONO formation and the rate of the heterogeneous dark reaction of NO_2 have the biggest influence on the system with a variation of around 10%. The effect of changes in the rate of the heterogeneous dark reaction within our experimental uncertainty is marked with a black square.

The reaction of OH with NO_2 represents an important radical sink in the system, especially in the beginning of the simulation, which could therefore have a significant impact on it. The reaction was identified as a major contributor to the uncertainty in the ethene photo-oxidation system (Zador et al., 2005). A reaction rate coefficient for the reaction of OH with NO_2 of 1.19×10^{-11} cm^3 molecule^{-1} s^{-1} (based on IUPAC, 2003) was used. A variation of this rate constant by ±15% (Fig. 9) changes the amount of TMB reacted after 400 min by ±9% under high NO_x conditions, but has a minor influence at higher VOC/NO_x (compared to a model measurement discrepancy of 100% under high NO_x conditions).

In several evaluations of the MCM using environmental chamber data it was shown that O(^{3}P) reactions with unsaturated organic compounds are important under chamber conditions, although they are not important for the ambient atmosphere (Hynes et al., 2005; Pinho et al., 2005, 2006) because the NO_x concentrations used in chambers are usually higher than those in the ambient atmosphere (<100 ppb, Jenkin, 2004). In addition to partially intercepting the formation of ozone, the reactions of O(^{3}P) with alkenes/etc are believed to lead to partial radical formation and could potentially have an influence on the radical balance in the system.

Therefore, O(^{3}P) reactions for TMB and for the main primary product methylglyoxal are included in the mechanism to test the influence on the TMB system. A reaction rate constant of 2.8×10^{-12} cm^3 molecule^{-1} s^{-1} (293K) was used (Calvert et al., 2002). According to Calvert (2002) the reaction leads to the formation of a phenolic product. The methylglyoxal reaction rate constant was estimated based on the OH rate constant to be 5×10^{-13} cm^3 molecule^{-1} s^{-1} (293 K) (Herron, 1988).

$$O(^3P)+1,3,5-\text{trimethylbenzene}=1,3,5-\text{trimethylphenol} \quad \text{(R1)}$$

$$O(^3P)+\text{methylglyoxal}=OH+CH_3CO_3 \quad \text{(R2)}$$

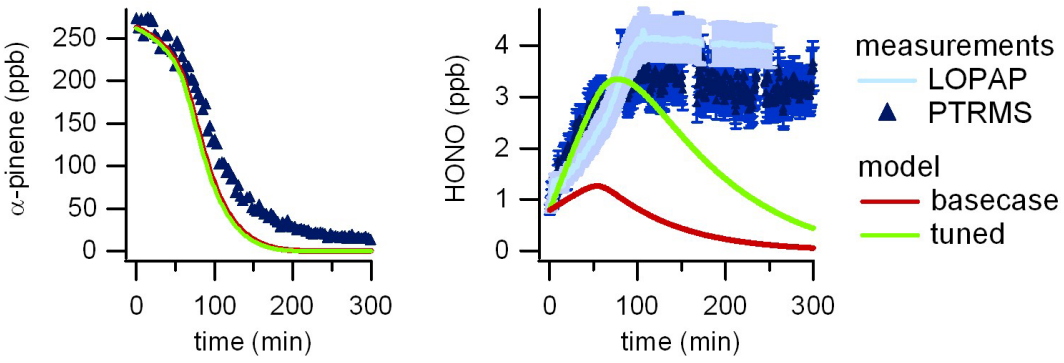

Fig. 10. Example plot of α-pinene photo-oxidation experiments, where HONO was measured with the LOPAP. The left panel shows the measured α-pinene concentration together with base (red) and tuned (green) model simulations. The right panel shows the HONO measured with the LOPAP and the model results. In addition, it shows results from a second experiment at similar conditions, where HONO was measured with the PTR-MS. The results from the two methods are in fairly good agreement. The discrepancies in the HONO concentration after around 120 min can be explained with slightly different NO_x input concentrations and a higher light intensity in the chamber during the experiment with the PTR-MS measurement leading to a lower HONO concentration due to the increased photolysis of HONO which is the main loss process. The fluctuations of the PTR-MS signal was mostly caused by instability sometimes occurring within the first 24 h after switching from normal to HONO measuring mode.

The inclusion of these reactions had a negligible effect on the simulations (<0.34% of TMB reacted for the 1200 ppb TMB experiments and no effect for experiments conducted at lower concentrations, see Fig. 9).

The uncertainties of single parameters are not sufficient to describe the observed discrepancy between measurement and model. A relatively good agreement could only be reached when all important parameters were biased in such a way that the TMB decay is maximized.

5.2 Nature of the light induced HONO formation as the missing OH radical source

In Figs. 3–5 it was clearly shown that the model is only able to simulate the TMB decay reasonably well when the uniform tuning reaction (NO_2+light/surface→HONO) is implemented into the mechanism. Very recently Li et al. (2008) determined new rate constants for a gas phase production of OH and HONO from the reaction of excited NO_2 with water. Implementing their mechanism into our model did only provide a negligible amount of additional HONO and OH reactivity. In the work of George et al. (2005) a photo-induced conversion of NO_2 into HONO was observed on organic films. It was shown that organic substrates containing a combination of electron donors, such as phenols, and of compounds yielding excited triplet states, such as aromatic ketones, showed a high reactivity towards NO_2. The resulting uptake coefficient of this light induced conversion exceeds that of the heterogeneous dark conversion by more than one order of magnitude. A similar light induced conversion of NO_2 into HONO on humic acid films and humic acid aerosol particles was observed by (Stemmler et al., 2006, 2007). In our experiments secondary organic aerosol (SOA) formation was followed using a scanning mobility particle sizer (Paulsen et al., 2005). Under low VOC-NO_x conditions (Figs. 3 and 4 left) SOA formation is suppressed by high NO_x concentrations throughout the first ~400 min of the experiment. Under medium VOC-NO_x (Figs. 3, 4 right and 5) conditions nucleation occurred typically after 120–200 min. The fact that HONO is already needed in the initial phase of the experiment when no secondary organic aerosol (SOA) is formed yet and under conditions where SOA formation is totally suppressed by high NO_x concentrations indicates that the aerosol pathway cannot be a dominant HONO source in our system. In the work of Bloss et al. (2005b) a conversion of NO_2 to HONO on SOA has been introduced to improve the model measurement agreement for toluene for a case study in the EUPHORE chamber. However, no experimental proof was given for the relatively high HONO concentrations that would be generated by such a reaction. They also stated that the reactive uptake coefficient required was much higher than the upper limit for such a dark process suggested by (Bröske et al., 2003).

A wall related reaction producing HONO is therefore more likely. This reaction would be in addition to the HONO formation included in the chamber auxiliary mechanism. Additional reactants (HC_{ad}) on the wall are needed to describe this extra NO_2 to HONO conversion. Considering the complex mixture of organics produced in these photochemical reactions it is well possible that photo-active compounds similar to humic acids deposit on the chamber walls. The overall reaction would then be in analogy to Stemmler et al. (2006):

$$NO_2 + (HC_{ad}) + \text{light/surface} = HONO + \text{products} \quad \text{(R3)}$$

Another possibility could be a reaction of nitric acid with organics on the chamber wall as speculated by Rohrer et al. (2005):

$$HNO_3 + (HC_{ad}) + \text{light/surface} = HONO + \text{products} \quad \text{(R4)}$$

In this work we implemented Reaction (R4) in a simplified way: first order dependence on NO_2 and no influence of organics (HC_{ad}). Although this simple tuning reaction led to a good agreement between modeled and measured TMB decay (Figs. 3–5) there occurs some deviation between measured and modeled HONO concentrations (Figs. 6 and 10). Based on our data it is not possible to clarify the nature of this light induced HONO production. A systematic investigation of the HONO evolution in these reaction systems is necessary to determine the responsible formation process. Based on these uncertainties it seems to be inevitable that HONO is measured during smog chamber experiments.

5.3 Ozone chemistry – NO_y-budget

As summarized from several chambers in Fig. A3 the model error in predicting the peak ozone concentration depends on the initial VOC/NO_x and the initial precursor concentration. It is most pronounced at medium VOC/NO_x and low precursor concentrations with ozone over-predictions up to 80%. This is directly linked to the NO_x chemistry and is reflected in the over-prediction of NO_2 as can be seen in the right panels of Figs. 3 and 4. Constraining the model with the measured NO_2 concentrations leads to a proper simulation of the ozone concentration.

Ozone production is determined by the ability of the mechanism in either converting NO to NO_2 or providing sinks of NO_x, such as HNO_3 and PAN, or peroxy radicals. As discussed in previous appraisals of aromatic mechanisms reducing the conversion of NO to NO_2 would result in a lower radical level and therefore in a lower oxidative capacity of the system. The implemented photo-enhanced conversion of NO_2 to HONO increases the reactivity due to the rapid photolysis of HONO. In addition this process converts NO_2 to NO without producing ozone. Therefore, this additional reaction is able to improve the ozone chemistry and even increases the radical level. Nevertheless, the tuned model still over-predicts the ozone formation at a later stage of the reaction. For further improvements of the mechanism measurements of NO_x sink species like HNO_3, PAN and organic nitrates are necessary.

5.4 Implications for other systems

Increased HONO concentrations in our smog chamber could also influence other systems which have been subject of recent mechanism evaluations (e.g. Pinho et al., 2005, 2006, 2007). While for the aromatics the MCM tends to underestimate the reactivity it tends to overestimate it for α-pinene (Pinho et al., 2007) and isoprene (Pinho et al., 2005). We also performed experiments with these two precursors and observed higher HONO concentrations than predicted by the respective MCM model for these systems too. As an example, α-pinene photo-oxidation experiments are shown in Fig. 10 where HONO was measured either with the LOPAP or with PTR-MS. The fluctuations of the PTR-MS signal was mostly caused by instability sometimes occurring within the first 24 h after switching from normal to HONO measuring mode. The mechanism was downloaded from the MCM website and $O(^3P)$ reactions were included as recommended from Pinho et al. (2007). Similar to the TMB system the tuning reaction has to be implemented to describe the higher observed HONO concentrations during these experiments. The simulations show that the influence of this light induced HONO formation on the predicted amount of α-pinene reacted is negligible. This is explained by the minor importance of HONO as a radical source compared to other reactions: the contribution of the HONO photolysis to the total new radical formation is only around 4%. However, the HONO concentration is not simulated well by the model, even with the tuned mechanism. Although the magnitude of HONO concentration is properly simulated, large deviations occur in the later stages of the experiment. This suggests again the simplified light induced NO_2 conversion as implemented here does not properly describe the system and that with increasing reaction time the light induced conversion of NO_2 to HONO is getting more efficient.

6 Conclusions

Consistent with previous appraisals of the aromatic mechanism as implemented in the MCM using chamber data, we found that the model significantly under-predicts the reactivity in the system. Higher measured than modeled HONO concentrations provide evidence for a light induced NO_2 to HONO conversion at the chamber walls, where the subsequent HONO photolysis explains the enhanced reactivity. This study shows the importance of HONO chemistry and the uncertainties introduced by surface reactions in smog chamber studies.

With the available dataset the exact mechanism of the photochemical source of HONO could not be constrained. It is expected that the source strength varies with the properties of the wall and thus the history of the chamber. Therefore, when using smog chamber data for the evaluation of chemical mechanisms, HONO measurements seem to be essential.

It was further shown that this increased HONO formation is not limited to TMB photo-oxidation. It is also observed in other chemical systems. However, the importance of HONO as a source of OH radicals may be less important as shown e.g. in the α-pinene photo-oxidation experiments and therefore the HONO chemistry is less obvious in this system.

By properly accounting for all chamber related reactions the aromatic mechanism as implemented in the MCM is able

to describe the measurements fairly well. Uncertainties remain with respect to the NO_x sinks.

Acknowledgements. The set of data from the SAPRC chambers was kindly provided by W. P. L. Carter. This work was supported by the Swiss National Science Foundation as well as the EC projects EUROCHAMP FP6-505968 and POLYSOA No 012719. We thank M. Jenkin for helpful discussions.

Edited by: A. Hofzumahaus

References

Bloss, C., Wagner, V., Bonzanini, A., Jenkin, M. E., Wirtz, K., Martin-Reviejo, M., and Pilling, M. J.: Evaluation of detailed aromatic mechanisms (MCMv3 and MCMv3.1) against environmental chamber data, Atmos. Chem. Phys., 5, 623–639, 2005a, http://www.atmos-chem-phys.net/5/623/2005/.

Bloss, C., Wagner, V., Jenkin, M. E., Volkamer, R., Bloss, W. J., Lee, J. D., Heard, D. E., Wirtz, K., Martin-Reviejo, M., Rea, G., Wenger, J. C., and Pilling, M. J.: Development of a detailed chemical mechanism (MCMv3.1) for the atmospheric oxidation of aromatic hydrocarbons, Atmos. Chem. Phys., 5, 641–664, 2005b, http://www.atmos-chem-phys.net/5/641/2005/.

Bröske, R., Kleffmann, J., and Wiesen, P.: Heterogeneous conversion of NO_2 on secondary organic aerosol surfaces: A possible source of nitrous acid (HONO) in the atmosphere?, Atmos. Chem. Phys., 3, 469–474, 2003, http://www.atmos-chem-phys.net/3/469/2003/.

Calvert, J. G., Atkinson, R., Becker, K. H., Kamens, R. M., Seinfeld, J. H., Wallington, T. J., and Yarwood, G.: The Mechanisms of Atmospheric Oxidation of Aromatic Hydrocarbons, Oxford University Press, Oxford, 556 pp., 2002.

Carter, W. P. L. and Lurmann, F. W.: Evaluation of a Detailed Gas-Phase Atmospheric Reaction-Mechanism Using Environmental Chamber Data, Atmospheric Environment Part a-General Topics, 25, 2771–2806, 1991.

Carter, W. P. L., Luo, D., Malkina, I. L., and Fitz, D.: The University of California, Riverside Environmental Chamber Data Base for Evaluating Oxidant Mechanisms. Indoor Chamber Experiments Through 1993, US Environmental Protection Agency, Research Triangle Park, NC, 1995a.

Carter, W. P. L., Luo, D., Malkina, I. L., and Pierce, J. A.: Environmental chamber studies of atmospheric reactivity of volatile organic compounds. Effects of varying chamber and light source. Final report to National Renewable Energy Laboratory, Contract XZ-2-12075, Coordinating Research Council, Inc., Project M-9, California Air Resources Board, Contract A032-0692, and South Coast Air Quality Management District, Contract C91323., 1995b.

Carter, W. P. L.: Documentation of the SAPRC-99 chemical mechanism for VOC reactivity assessment. Final Report to California Air Resources Board Contract 92-329 and Contract 95-308, Air Pollution Research Center and College of Engineering Center for Environmental Research and Technology University of California Riverside, California, 2000.

Carter, W. P. L., Cocker, D. R., Fitz, D. R., Malkina, I. L., Bumiller, K., Sauer, C. G., Pisano, J. T., Bufalino, C., and Song, C.: A new environmental chamber for evaluation of gas-phase chemical mechanisms and secondary aerosol formation, Atmos. Environ., 39, 7768–7788, 2005.

Derwent, R. G., Davies, T. J., Delaney, M., Dollard, G. J., Field, R. A., Dumitrean, P., Nason, P. D., Jones, B. M. R., and Pepler, S. A.: Analysis and interpretation of the continuous hourly monitoring data for 26 C-2-C-8 hydrocarbons at 12 United Kingdom sites during 1996, Atmos. Environ., 34, 297–312, 2000.

Finlayson-Pitts, B. J., Wingen, L. M., Sumner, A. L., Syomin, D., and Ramazan, K. A.: The heterogeneous hydrolysis of NO2 in laboratory systems and in outdoor and indoor atmospheres: An integrated mechanism, PCCP Phys. Chem. Chem. Phys., 5, 223–242, 2003.

George, C., Strekowski, R. S., Kleffmann, J., Stemmler, K., and Ammann, M.: Photoenhanced uptake of gaseous NO2 on solid-organic compounds: a photochemical source of HONO?, Faraday Discussions, 130, 195–210, 2005.

Gutzwiller, L., Arens, F., Baltensperger, U., Gaggeler, H. W., and Ammann, M.: Significance of semivolatile diesel exhaust organics for secondary HONO formation, Environ. Sci. Technol., 36, 677–682, 2002.

Hak, C., Pundt, I., Trick, S., Kern, C., Platt, U., Dommen, J., Ordonez, C., Prevot, A. S. H., Junkermann, W., Astorga-Llorens, C., Larsen, B. R., Mellqvist, J., Strandberg, A., Yu, Y., Galle, B., Kleffmann, J., Lorzer, J. C., Braathen, G. O., and Volkamer, R.: Intercomparison of four different in-situ techniques for ambient formaldehyde measurements in urban air, Atmos. Chem. Phys., 5, 2881–2900, 2005, http://www.atmos-chem-phys.net/5/2881/2005/.

Healy, R. M., Wenger, J. C., Metzger, A., Duplissy, J., Kalberer, M., and Dommen, J.: Gas/particle partitioning of carbonyls in the photooxidation of isoprene and 1,3,5-trimethylbenzene, Atmos. Chem. Phys., 8, 3215–3230, 2008, http://www.atmos-chem-phys.net/8/3215/2008/.

Heland, J., Kleffmann, J., Kurtenbach, R., and Wiesen, P.: A new instrument to measure gaseous nitrous acid (HONO) in the atmosphere, Environ. Sci. Technol., 35, 3207–3212, 2001.

Herron, J. T.: Evaluated Chemical Kinetic Data for the Reactions of Atomic Oxygen O(3P) with Saturated Organic-Compounds in the Gas-Phase, J. Phys. Chem. Ref. Data, 17, 967–1026, 1988.

Hynes, R. G., Angove, D. E., Saunders, S. M., Haverd, V., and Azzi, M.: Evaluation of two MCMv3.1 alkene mechanisms using indoor environmental chamber data, Atmos. Environ., 39, 7251–7262, 2005.

Jenkin, M. E., Saunders, S. M., and Pilling, M. J.: The tropospheric degradation of volatile organic compounds: a protocol for mechanism development, Atmos. Environ., 31, 81–104, 1997.

Jenkin, M. E., Saunders, S. M., Wagner, V., and Pilling, M. J.: Protocol for the development of the Master Chemical Mechanism, MCM v3 (Part B): tropospheric degradation of aromatic volatile organic compounds, Atmos. Chem. Phys., 3, 181–193, 2003, http://www.atmos-chem-phys.net/3/181/2003/.

Jenkin, M. E.: Modelling the formation and composition of secondary organic aerosol from alpha- and beta-pinene ozonolysis using MCM v3, Atmos. Chem. Phys., 4, 1741–1757, 2004, http://www.atmos-chem-phys.net/4/1741/2004/.

Kelly, T. J., and Fortune, C. R.: Continuous Monitoring of Gaseous Formaldehyde Using an Improved Fluorescence Approach, Int. J. Environ. An. Ch., 54, 249–263, 1994.

Killus, J. P. and Whitten, G. Z.: Background Reactivity in Smog Chambers, Int. J. Chem. Kinet., 22, 547–575, 1990.

Kleffmann, J., Heland, J., Kurtenbach, R., Lorzer, J., and Wiesen, P.: A new instrument (LOPAP) for the detection of nitrous acid (HONO), Environ. Sci. Pollut. R., 48–54, 2002.

Kleffmann, J., Lorzer, J. C., Wiesen, P., Kern, C., Trick, S., Volkamer, R., Rodenas, M., and Wirtz, K.: Intercomparison of the DOAS and LOPAP techniques for the detection of nitrous acid (HONO), Atmos. Environ., 40, 3640–3652, 2006.

Lanz, V. A., Alfarra, M. R., Baltensperger, U., Buchmann, B., Hueglin, C., and Prevot, A. S. H.: Source apportionment of submicron organic aerosols at an urban site by factor analytical modelling of aerosol mass spectra, Atmos. Chem. Phys., 7, 1503–1522, 2007,
http://www.atmos-chem-phys.net/7/1503/2007/.

Li, S. P., Matthews, J., and Sinha, A.: Atmospheric hydroxyl radical production from electronically excited NO_2 and H_2O, Science, 319, 1657–1660, 2008.

Molina, L. T., Kolb, C. E., de Foy, B., Lamb, B. K., Brune, W. H., Jimenez, J. L., Ramos-Villegas, R., Sarmiento, J., Paramo-Figueroa, V. H., Cardenas, B., Gutierrez-Avedoy, V., and Molina, M. J.: Air quality in North America's most populous city – overview of the MCMA-2003 campaign, Atmos. Chem. Phys., 7, 2447–2473, 2007,
http://www.atmos-chem-phys.net/7/2447/2007/.

Paulsen, D., Dommen, J., Kalberer, M., Prevot, A. S. H., Richter, R., Sax, M., Steinbacher, M., Weingartner, E., and Baltensperger, U.: Secondary organic aerosol formation by irradiation of 1,3,5-trimethylbenzene-NO_x-H_2O in a new reaction chamber for atmospheric chemistry and physics, Environ. Sci. Technol., 39, 2668–2678, 2005.

Pinho, P. G., Pio, C. A., and Jenkin, M. E.: Evaluation of isoprene degradation in the detailed tropospheric chemical mechanism, MCM v3, using environmental chamber data, Atmos. Environ., 39, 1303–1322, 2005.

Pinho, P. G., Pio, C. A., Carter, W. P. L., and Jenkin, M. E.: Evaluation of alkene degradation in the detailed tropospheric chemistry mechanism, MCM v3, using environmental chamber data, J. Atmos. Chem., 55, 55–79, 2006.

Pinho, P. G., Pio, C. A., Carter, W. P. L., and Jenkin, M. E.: Evaluation of alpha- and beta-pinene degradation in the detailed tropospheric chemistry mechanism, MCM v3.1, using environmental chamber data, J. Atmos. Chem., 57, 171–202, 2007.

Rohrer, F., Bohn, B., Brauers, T., Bruning, D., Johnen, F. J., Wahner, A., and Kleffmann, J.: Characterisation of the photolytic HONO-source in the atmosphere simulation chamber SAPHIR, Atmos. Chem. Phys., 5, 2189–2201, 2005,
http://www.atmos-chem-phys.net/5/2189/2005/.

Saunders, S. M., Jenkin, M. E., Derwent, R. G., and Pilling, M. J.: Protocol for the development of the Master Chemical Mechanism, MCM v3 (Part A): tropospheric degradation of non-aromatic volatile organic compounds, Atmos. Chem. Phys., 3, 161–180, 2003a,
http://www.atmos-chem-phys.net/3/161/2003/.

Saunders, S. M., Pascoe, S., Johnson, A. P., Pilling, M. J., and Jenkin, M. E.: Development and preliminary test results of an expert system for the automatic generation of tropospheric VOC degradation mechanisms, Atmos. Environ., 37, 1723–1735, 2003b.

Steinbacher, M., Dommen, J., Ammann, C., Spirig, C., Neftel, A., and Prevot, A. S. H.: Performance characteristics of a proton-transfer-reaction mass spectrometer (PTR-MS) derived from laboratory and field measurements, Int. J. Mass Spectrom., 239, 117–128, 2004.

Stemmler, K., Ammann, M., Donders, C., Kleffmann, J., and George, C.: Photosensitized reduction of nitrogen dioxide on humic acid as a source of nitrous acid, Nature, 440, 195–198, 2006.

Stemmler, K., Ndour, M., Elshorbany, Y., Kleffmann, J., D'Anna, B., George, C., Bohn, B., and Ammann, M.: Light induced conversion of nitrogen dioxide into nitrous acid on submicron humic acid aerosol, Atmos. Chem. Phys., 7, 4237–4248, 2007,
http://www.atmos-chem-phys.net/7/4237/2007/.

Takeuchi, M., Li, J. Z., Morris, K. J., and Dasgupta, P. K.: Membrane-based parallel plate denuder for the collection and removal of soluble atmospheric gases, Anal. Chem., 76, 1204–1210, 2004.

Wagner, V., Jenkin, M. E., Saunders, S. M., Stanton, J., Wirtz, K., and Pilling, M. J.: Modelling of the photooxidation of toluene: conceptual ideas for validating detailed mechanisms, Atmos. Chem. Phys., 3, 89–106, 2003,
http://www.atmos-chem-phys.net/3/89/2003/.

Wisthaler, A., Hansel, A., Jordan, A., and Märk, T. D.: Recent Developments in Proton-Transfer- Reaction Mass Spectrometry, in: Proceedings to the XXIV International Conference, Photonic, Electronic and Atomic Collisions, Rosario, Argentina, 462–469, 2005.

Yu, J. Z. and Jeffries, H. E.: Atmospheric photooxidation of alkylbenzenes. 2. Evidence of formation of epoxide intermediates, Atmos. Environ., 31, 2281–2287, 1997.

Zador, J., Wagner, V., Wirtz, K., and Pilling, M. J.: Quantitative assessment of uncertainties for a model of tropospheric ethene oxidation using the European Photoreactor (EUPHORE), Atmos. Environ., 39, 2805–2817, 2005.

Zador, J., Turanyi, T., Wirtz, K., and Pilling, M. J.: Measurement and investigation of chamber radical sources in the European Photoreactor (EUPHORE), J. Atmos. Chem., 55, 147–166, 2006.